Title

Stress and Distortion of 100Cr6 Steel after Quenching in Aqueous 4% Polyvinylpyrrolidone Solution

Author(s)

Xuan Thi Tran , Pham Hoang Anh, Vuong Van Hoang, Toai Dinh Vu

Journal

Journal of Materials Engineering and Performance

Volume 31, pp. 6672-6688, 2022

Published

2022-02-28

URL

https://link.springer.com/article/10.1007/s11665-022-06726-3

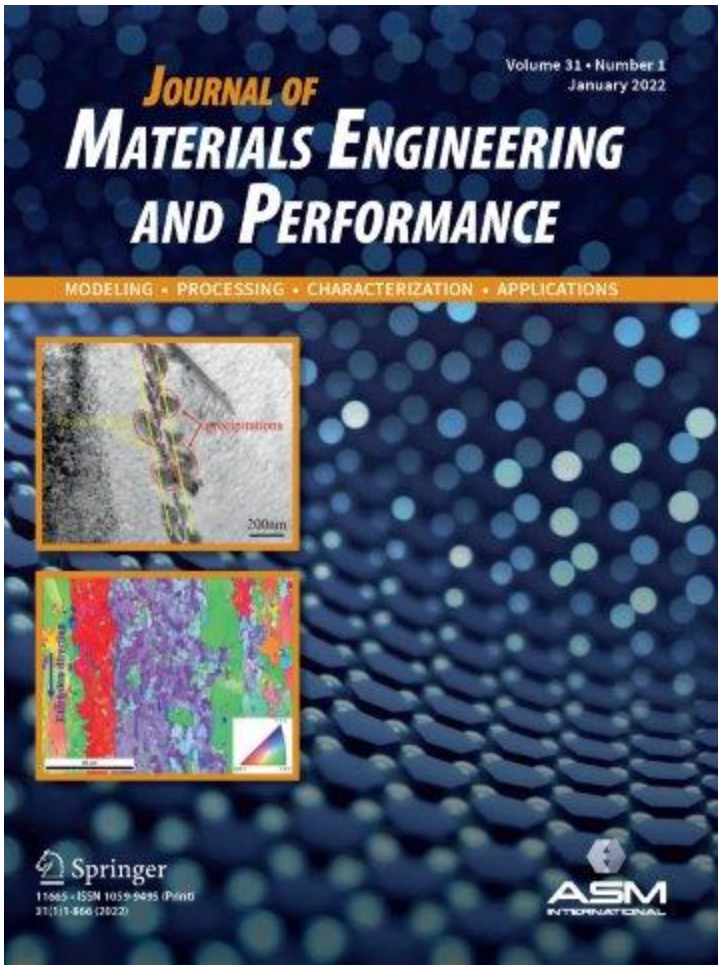

Stress and distortion of 100Cr6 steel after quenching in aqueous 4% polyvinylpyrrolidone solution

Journal:	*Journal of Materials Engineering and Performance*
Manuscript ID	JMEP-21-10-25768.R1
Manuscript Type:	Technical Article
Date Submitted by the Author:	24-Jan-2022
Complete List of Authors:	Vu, Toai; Hanoi University of Science and Technology, School of Mechanical Engineering Tran, Xuan; Hanoi University of Science and Technology, School of Materials Science and Engineering Pham, Anh; Shimane University Hoang, Vuong; Hanoi University of Science and Technology
Keywords:	PVP, quenching, 100Cr6, stress, distortion

Stress and distortion of 100Cr6 steel after quenching in aqueous 4% polyvinylpyrrolidone solution

Xuan Thi Tran[1)], Anh Hoang Pham[2)], Vuong Van Hoang[1)], Toai Dinh Vu[3)] *

1) School of Materials Science and Engineering, Hanoi University of Science and Technology, 1 Dai Co Viet Road, Ha Noi, Viet Nam.

2) Department of Physics and Materials Science, Shimane University, 1060 Nishikawatsu-cho, Matsue, Shimane 690-8504, Japan.

3) School of Mechanical Engineering, Hanoi University of Science and Technology, 1 Dai Co Viet Road, Ha Noi, Viet Nam.

E-mail: xuan.tranthi@hust.edu.vn, anhpham@riko.shimane-u.ac.jp, vuong.hoangvan@hust.edu.vn

*Corresponding Author: toai.vudinh@hust.edu.vn

Received xxxxxx

Accepted for publication xxxxxx

Published xxxxx

Abstract

The stress and distortion that remains in steel products after quenching are harmful and undesirable. Therefore, a selected quenching medium should have a cooling rate equal to or greater than the critical cooling rate of the steel to achieve high hardness values, but the cooling rate should not be too large in order to minimize stress and distortion on the specimen. This paper studied the hardness, stress, and distortion of C-ring samples quenched in 4% polyvinylpyrrolidone (PVP) – K60 solution and oil using simulated and experimental measurements. The results show that the maximum cooling rates (CR_{max}) of oil and 4% PVP-K60 quenchants are both higher than the critical cooling rate of steel. The CR_{max} of the 4% PVP-K60 solution is greater than that of the oil, and the cooling rate of the 4% PVP-K60 solution at 300 °C (CR_{300}) is smaller than that of the oil. The greater the CR_{300} is, the greater the hardness, stress, and distortion are. Thus, the hardness, stress, and distortion values of the quenched sample depend less on CR_{max} and more on CR_{300}. The research results also showed that a solution of 4% PVP-K60 could replace oil in the quenching of 100Cr6 steel. Simulated and experimental results of the hardness, stress, and distortion of C-ring samples reflected the same rule. The errors between the simulation and experiment using the program and the computational conditions of distortion are approximately 20%. The numerical simulation method is entirely usable to predict the hardness, stress, and distortion of a sample during the quenching process.

KEY WORDS: PVP, quenching, 100Cr6, stress, distortion

1. Introduction

Most types of steel, including carbon, low-alloy and tool steels, are quenched to produce controlled amounts of martensite in their microstructures. Successful hardening usually means achieving the required microstructure, hardness, strength, or toughness while minimizing the residual stress, distortion, and possibility of cracking (Ref 1).

During the steel quenching process, complex thermal behaviors produce significant thermal residual stresses, leading to cracking and distortion. In many other cases, high residual stress is the main cause of reductions in the the functional abilities and lifetimes of steel parts even in the absence of cracks (Ref 2-4). Therefore, the determination of the internal stress in steel parts is a critical and necessary task. The known residual stress value is a useful factor for optimizing the parameters of the fabrication process and heat treatment in both science and practice.

Considering the phase transformation during the quenching of metal, the stress of steel parts is formed due to two primary reasons: "thermal stress" (the difference in the temperature between the surface and bulk of steel parts after

quenching) and "phase stress" (the change in the volume of the lattice due to the phase transformation). In steel, the specific volume of martensite (body-centered tetragonal) is higher than that of austenite (face-centered cubic). Therefore, the austenite-to-martensite transformation causes an increase in the lattice volume, which contributes significantly to the distortion and residual stresses in quenched steel parts.

If choosing the proper quenchant, the minimization of the distortion and residual stresses in steel parts can be achieved while still ensuring the mechanical requirements (Ref 5). Oil quenchants have been the most frequently used in the heat treatment industry, particularly for crack-sensitive steel parts. Oil, however, has several substantial disadvantages: relatively limited variabilities in quench rates, fire hazards, and smoke emissions (Ref 6). The cooling power of polymers that are used as quenching fluids has been studied by varying experimental parameters such as polymer concentration, the molecular weight of the polymer, bath temperature, and agitation (Ref 7-8). Thus, aqueous polymer quenchants have been developed to replace oil solutions in some applications and fill the gap between the cooling rates of water and oils (Ref 6-8). Polymer quenchants are economical, nonflammable, easy to clean, and have a wide range of cooling rates (Ref 8).

PVP solution has been studied as a quenchant since 1975 and has high solubility in water, and it is evaluated as a more stable quenchant than oil (Ref 9). There are five common types of PVP on the market (PVP K-15, PVP K-30, PVP K-60, PVP K-90, and PVP K-120) with a molecular weight range of 2500-3000000 g/mol.

Polyvinylpyrrolidone (PVP) is a biodegradable, water-soluble polymer. To promote the decomposition of PVP, some enzymes, such as gamma-lactamase and amidase, are used to degrade PVP molecules or to absorb activated sludge. Therefore, PVP quenchant solution is safe and friendly with regard to the environment (Ref 10). Eduardo Vieiraat et al. (Ref 11) researched the microstructural characteristics and properties of AISI 1045 steel quenched in solutions of polyvinylpyrrolidone (PVP) with concentrations of 10, 15, 20, and 25%. Microstructural characterization quantified the percentages of the crystalline phases generated by each of the concentrations of the PVP quenching solutions, demonstrating a reduction in martensite at high concentrations (Ref 10). The stress and distortion of the samples was not considered. A Zainulabdeen et al. (Ref 12) studied the effect of PVP quenching media on mechanical CK45 steel. The results show that 20% PVP at 40 °C can be used instead of water in the quenching and tempering treatment for medium carbon steel samples, thereby reducing the overall cost of the heat treatment process of medium carbon steel (Ref 12).

To select a proper PVP quenchant to replace an oil quenchant for a specific steel, it is necessary to evaluate the distortion and residual stresses in the parts after quenching using standard C-ring samples. The experimental evaluation of distortion and residual stresses is time-consuming and difficult, especially when many variations of the PVP quenchants

should be considered. To overcome the disadvantages of this experimental method, a simulation method of metal heat treatment is currently a promising approach.

Some authors have studied the simulation of heat treatment, but simulations of fully mechanical, physical and metallurgical behavior are scarce because of the limitations of the simulation software and computer capacities. Hernandez-Morales et al. (Ref 13) applied an uncoupled thermoelastoplastic model to predict the internal stress field and distortion of AISI 304 stainless steel C-rings upon quenching. DEFORM-HT (commercial software) was used for the calculations, which did not consider any phase transformations. The simulations showed that distortion occurs initially due to the thermal contraction of the probe tip followed by the thermal contraction of the medium portion of the probe arm. Nailu Chen et al. (Ref 14) simulated the quenching process of 42CrMo steel connecting rods in oil and aqueous polyalkylene-glycol (PAG) solutions using the commercial finite element software MSC Marc. According to the calculated immersion time, the as-forged connecting rods were quenched in 14% aqueous PAG solution, and the resultant mechanical properties were higher than the requirements. Meanwhile, cracking was prevented completely. These results indicate that the calculated results conformed to the experimental results. However, the calculation and evaluation of the residual stress and distortion on samples cooled in oil and PAG solution were not performed.

The current state of simulations of the heat treatment process requires improving the simulation consistency and reducing the gap between simulation and experimental measurements. In this study, the software SYSWELD from ESI Groups was used, which can fully consider the mechanical, physical, thermal and metallurgical behaviors in the simulation of the quenching process to evaluate the residual stress and distortion of the C-ring shaped model. A new construction of the model's surface was also considered to address the very high heat transfer rate during the quenching process.

This paper focuses on evaluating the residual stress and distortion in C-ring samples of 100Cr6 steel after quenching in a 4% PVP-K60 solution by numerical simulation calculations and experiments. 100Cr6 steel is a typical bearing steel that is typically quenched in oil (Ref 15, 16), but here, a 4% PVP-K60 quenchant was selected as an environmentally friendly replacement for oil. The simulation results conform well to the experimental results, as the discrepancy between the simulation and experimental results of the residual stress and distortion are small.

2. Numerical Simulation

2.1. Modeling of the quenching process

A C-ring sample is commonly used to study the distortion of steel parts after heat treatment (Ref 17-19). Because of the differences in thickness, angle (acute or obtuse) and gap width, many factors can be studied during quenching, such as heat

transfer, phase transformation, hardness, stress, and distortion. In this study, the shape and size of the C-ring sample are shown in **Fig. 1a**.

(Fig. 1)

The cross-section of the C-ring sample is shown in **Fig. 1a**. A design of a 3D model with a 20 mm height was carried out by SolidWorks 2016 software. The requirements of the 3D model are formatted in *.IGS to be compatible with the finite element model in the Visual-Mesh module of SYSWELD software.

Free mesh is the most suitable for models that have different shapes and sizes (Ref 20). To divide the free mesh of the model's shell, the authors chose a quadratic triangle element in order to prevent the nonfilling of the model and thus ensure calculation accuracy (Ref 21). To overcome the heat transfer problem of a very high-temperature gradient, such as in quenching (the difference in temperature between the surface of the model and the inner layer is very large), the material close to the high-temperature gradient areas was meshed into thin layers to obtain calculation results with high accuracy (finer meshing in the increasing direction of the temperature gradient) (Ref 22). On the other hand, the finite element method requires that the nodes at the model's surface coincide with the adjacent nodes in the inner region. To ensure this, the authors chose a triangular prism element to mesh five layers near the shell and a 4-node tetrahedral element to mesh the model's core. If choosing incompatible element types, some nodes on the model's shell will not coincide with nodes in the inner region, and the calculation will fail - this is critical to note when calculating by the finite element method.

It is also critical to note for the finite element method that if the model is divided into a finer mesh, the obtained results are more precise, but it takes a longer calculation time and more computer memory. Bathe (Ref 23) stated that the accuracy of the finite element method increases when the element size is smaller. However, when the size of the elements is decreased to a certain extent, then the precision of the computation's accuracy barely increases (or does not increase at all), while the computation quantity increases dramatically, resulting in a time-consuming process that utilizes much computer memory. To ensure the optimization of computational time and storage and obtain the necessary accurate results, the author conducted simulation tests with the same optimized shape and dimensions while varying the size of the element. The simulation results show that the model with the longest edge (2 mm) is the best choice because its computation produced high accuracy and reduced the usage of computer memory storage and time.

The Visual-Mesh 13.0 module of the SYSWELD software is used to mesh the model with the above chosen elements and requirements, and the finite element model is obtained as shown in **Fig. 1b**. The meshing of the 2 mm long edge on the

surface of model by a quadratic triangle element will first build the skin of the model, then the layers that are near the shell will be meshed by the "mesh layer" function of the Visual-Mesh module by a triangular prism element (the 0.5 mm thick material layer will be divided into 5 layers that increase in thickness from the outside of the shell towards the inside). The thickness of the innermost layer is three times higher than that of the outermost layer. Specifically, the thicknesses of the 5 layers of the shell are 0.05, 0.075, 0.1, 0.125 and 0.15 mm. Finally, the inner core of the model was meshed by a 4-node tetrahedral element with the top edge of the element set at 2 mm. The final model has a total of 54019 elements with 18026 nodes. This meshing method applied in SYSWELD is a new technique (since version 2017) to improve simulation accuracy.

2.2. Assignment of the material properties

The FEM model, as shown in **Fig. 1b,** must have clearly defined material properties. This means that a full set of physical material properties must be assigned. In this study, 100Cr6 steel was used, which has the following physical properties: thermal conductivity, specific heat, yield strength, and Young's modulus (Ref 20).

2.3. Calculational conditions for the simulation of the quenching process.

Heat transfer conditions between the model and a quenchant

It can be assumed that heat flow during quenching occurs by two distinct mechanisms:

a) The heat flows through the internal region by a thermal conduction mechanism – this is represented by the thermal conductivity coefficient K [W/mmK]

b) The heat flows from the model to the quenchant by a thermal convection mechanism – this is represented by the heat transfer coefficient HTC [W/mm^{2}K].

In the numerical simulation, the heat transfer process from the surface or shell of the simulation model to the quenchant is characterized by 2D elements that are meshed and assigned before calculation (**Fig. 2a**). The heat transfer coefficient (HTC) of the model's shell is the boundary condition of the simulation in the quenching process. Therefore, it has to be assigned to the model during the establishment of the simulation parameters. To determine the heat transfer coefficient (HTC) of the quenching solution in order to provide the input data for the numerical simulation, the authors conducted an experiment to measure the cooling curves according to ISO 9950:1995 with a standard sample of Inconel 600. From the measured cooling curves, the cooling rate curves of the quenchant were determined, which allowed for the calculation of

the heat transfer coefficient of the quenching medium by the HTC calibration function of SYSWELD. The HTC coefficient was added to the SYSWELD 2017.0 software for the simulation of specific models.

As a result, the HTC values of the 4% PVP – K60 and oil quenchants are a function of temperature (**Fig. 2b)**. When the quenching temperature is high (vapor film stage) or the cooling temperature is close to the quenchant temperature (convection stage), the HTC of the quenchant is small, whereas this value is very high in the boiling stage.

(Fig. 2)

Sample clamping conditions during quenching

In addition to the boundary condition of the HTC between the model and quenchant, the clamping method and position and the immersion method of the sample in the quenchant are also important boundary conditions that need to be correctly assigned when setting the simulation parameters. In this study, the C-ring sample is vertically clamped on two planes and embedded in the Y-axis, as shown in **Fig. 3a**. The clamping method and position influence the stress and distortion of the sample during quenching. With a constant quenchant type and sample shape, if the clamping method and position are not appropriate, a reduction in the working ability of the sample will be caused by the resulting high distortion and residual stress, which can even result in the waste of the sample after quenching.

(Fig. 3)

Quenching parameters

To simulate the quenching process of the finite element model, parameters such as the material properties, heat transfer conditions, and sample clamping method will be assigned and set in the SYSWELD 2017.0 software. In addition, other parameters are also considered in the calculation shown in **Table 1**. These parameters are set as the "input parameters" of the numerical simulation process. First, the C-ring sample is meshed into the finite element model by the Visual-Mesh module, and then the heat transfer of the quenching process is simulated by a Visual-Heat Treatment calculation module after setting the input parameters such as the mechanical, thermal and metallic properties of 100Cr6 steel.

(Table 1)

3. Materials and Methods

3.1. Materials and sample preparation

The material employed for the C-ring specimen was 100Cr6 steel (DIN 17230) with a nominal chemical composition (certified by the supplier) of 1.04% C, 0.26% Si, 0.33% Mn, 0.31% Ni, 1.53% Cr, and 0.01% Mo. The imported steel is precleaned and stored and then cut into a C-ring pattern with the correct dimensions by wire electric discharged machining, as shown by the simulated models in **Fig. 1a**. After cutting, the sample was degreased, ground with sandpaper (100, 240, 400, 600, 800, and 1000) and polished with 3 μm Al_2O_3 powder to eliminate undulations on the surface.

3.2. Quenching process

The C-ring specimen was heated to 850 °C in a Nabertherm N11/H furnace (Germany) and held at this temperature for 1800 seconds to ensure that the sample was completely austenitic. Then, the sample was quenched in the 4% PVP - K60 solution and oil with a soaking time of 500 seconds to ensure that the sample was cooled to ambient temperature. In this paper, 100Cr6 steel was quenched in a 4% PVP-K60 solution because the measured cooling rate of this quenchant is equivalent to oil. In addition, the cooling characteristics also show that the 4% PVP-K60 solution is better than oil - this is clearly analyzed in the results section of this paper.

3.3. Hardness measurements after quenching

After quenching in the 4% PVP - K60 solution and oil, the C-ring samples were cut into two equal parts to study their hardness. Then, the samples were ground at their cross-sections with sandpaper (100, 240, 400, 600, and 1000) and polished by 3 μm Al_2O_3 powder, and their hardness was measured by a Duramin-2 machine.

3.4. Residual stress measurements

In the early 20th century, X-rays began to be used to determine the stress of crystals. In 1961, Mchearauch proposed the $\sin^2\psi$ method for X-ray stress measurements. Currently, XRD is the most widely used stress measurement method and has been applied in various measurement fields. The principle of the stress measurement method is specified in the appendix (Ref 21, 24-26).

The authors of this paper used the X-ray diffraction method for measuring the residual stress with a D/MAX RAPID II Rigaku. The mechanical properties of the 100Cr6 steel that were necessary to assign before using the device included the elastic modulus (E = 200 GPa) and the Poisson coefficient (ν = 0.28) (according to ASTM A295 standard). The angle ψ between the incident beams and the axis of σ_3 or ε_3 was adjusted to be in the range of 0° to 45° [27]. Five diffraction images with various ψ orientations were taken in this study.

3.5. Distortion measurements

The distortion of the C-rings is usually examined through the changes in the dimensional measurements of the inner diameter (ID) and outer diameter (OD), gap width (GW), thickness, flatness, cylindricity and roundness. In this study, the dimensions (m, a and n) of the sample are measured by using a coordinate measuring machine. The changes in the ID, OD and GW characterize the distortion of the sample (Ref 28-30). The GW was measured at the top, middle, and bottom of the sample (**Fig. 3b**).

For the study of distortion, C-ring samples were prepared according to the following procedure:

+ Step 1: The samples were ground and polished before quenching.

+ Step 2: The dimensions (m, a and n) of the C-ring samples were measured before heat treatment (**Fig. 3b**) by a Profile Projector coordinate measuring machine.

+ Step 3: The samples were heated in a N11/H furnace and quenched following the procedure**.**

+ Step 4: The Profile Projector also provides preliminary cleaning and measures the n', m', a' of the samples after quenching (**Fig. 3b)**. The GWs, IDs, and ODs of the samples were calculated according to the following equations:

$$\mathbf{GW = n' - n.} \quad (1)$$

$$\mathbf{ID = a' - a.} \quad (2)$$

$$\mathbf{OD = m' - m.} \quad (3)$$

4. Results and discussion

4.1. Cooling capacity difference of the 4% PVP-K60 and oil quenchants

By analyzing the cooling curve, it is possible to elucidate the cooling capacity of the quenching medium, the tendency for vapor film appearance and the cooling rate at lower temperatures during the formation of martensite. The cooling curve gives an immediate picture of the characteristics of the quenchant and makes it easy to compare the used quenchant with a newly mixed quenchant to identify possible changes in the cooling capacity. Many characteristics can be recorded or calculated, such as the maximum cooling rate (CR_{max}), the temperature at which the maximum cooling rate occurs, the cooling rate at 300 °C (CR_{300}) and cooling times under certain temperatures (e.g., 600, 400 and 200 °C) (Ref 9, 31). Two of the more common parameters obtained from cooling curves are CR_{max} and CR_{300}. Usually, it is desirable for CR_{max} to occur at higher temperatures in the ferrite and pearlite transformation region if the maximum hardness is desired because this

minimizes ferrite and pearlite formation. The cooling rates in the region where martensite starts to form from austenite, Ms, should be minimized to reduce the potential for cracking and distortion (Ref 1). **Fig. 4** shows the measured cooling curves and cooling rates of the 4% PVP - K60 solution and oil according to ISO 9950.

The results show that the CR_{max} of the 4% PVP-K60 solution is greater than that of the oil, but the CR_{300} of the 4% PVP-K60 solution is lower than that of the oil. Specifically, the 4% PVP-K60 solution had a maximum cooling rate of 87 °C/s, which was higher than that of the oil (80 °C/s), while the CR_{300} values of the 4% PVP-K60 and oil quenchants was 14.5 and 30 °C/s, respectively. Thus, the 4% PVP-K60 quenchant was selected when quenching steel parts with complex shapes made from high carbon steel or alloy steel to minimize the generation of distortion and stress.

(Fig. 4)

From the cooling rate results in **Fig. 4b**, the HTC values of the 4% PVP-K60 and oil quenchants were calculated according to the literature (Ref 32-35). These HTC values, as shown in **Fig. 2b,** were used as input parameters in the simulation process of 100Cr6 steel quenching in 4% PVP-K60 and oil quenchants. The hardness, stress and distortion results are shown in the following sections.

4.2. Numerical simulation results

4.2.1. Hardness of the C-ring sample after quenching in 4% PVP-K60 and oil quenchants

By calculating the hardness of the sample while simultaneously calculating the stress and deformation when quenching in 4% PVP-K60 and oil quenchants, we obtain the results shown in **Fig. 5**.

(Fig. 5)

The results of the hardness calculation of the oil-quenched sample in **Fig. 5a** show that the highest hardness of the specimen is 778.263 HV at the top position of the C-ring (node 1177), where the thickness is the smallest and the cooling rate is the largest. At node 3360 (the core of the C-ring), the lowest hardness is 775.039 HV, corresponding to the location with the lowest cooling rate. The image of the color band distribution in **Fig. 5a** shows that the thinnest part of the C-ring sample has the greatest hardness, and the hardness values decrease from the thinnest to the thickest part and from the surface to the core of the C-ring sample. This result also reflects the theory of the quenching process: at a location with a

higher cooling rate, the hardness is higher (Ref 1, 36). However, the difference in the hardness values at node 1177 (the C-ring top) and node 3660 (in core) was only approximately 3.2 HV.

The calculation results in **Fig. 5b** show that after 500 seconds of quenching in the 4% PVP-K60 solution, node 1177 at the top of the C-ring exhibited a maximum hardness of 777.143 HV and the minimum hardness is 772.959 HV at node 1996 (in the core of the model). The hardness distribution results of the C-ring quenched in the 4% PVP-K60 solution were similar to those of the C-ring quenched in the oil: locations in the thinner region have greater hardness due to the larger cooling rate, and the hardness values decrease from the thinnest to the thickest part and from the surface to the core of the C-ring sample. The difference in hardness between node 1177 (the top of the C-ring) and node 1996 (in the core) is only 4.2 HV. The results of the hardness simulation shown in **Fig. 5** also confirm that when the C-ring samples were quenched in the 4% PVP-K60 solution and oil (their cooling rate is described in **Fig. 4**), the cooling rate at the core of the C-ring was more significant than the critical cooling rate of the 100Cr6 steel (approximately 40 °C/s) (**Fig. 6**). In other words, the C-ring was quenched completely in both 4% PVP-K60 and oil quenchants. In particular, the difference in hardness when quenching in oil and 4% PVP-K60 is not significant (only 1.12 HV at the tip and 2.08 HV at the core), which means that 4% PVP-K60 can be used instead of oil as the quenching medium without significantly affecting the resulting hardness of the 100Cr6 steel.

(Fig. 6)

4.2.2. Stress fields in the C-ring samples after quenching

The calculated results of the stress components in the C-ring samples after quenching in the 4% PVP-K60 solution are shown in **Figs. 7** and **8**. The SYSWELD software conventions are such that positive stress is the tensile stress and negative stress is the compression stress and has the minus sign "-" before the value in the scale.

(Fig. 7)

Fig. 7 shows the calculated von Mises residual stress field (σeqv) and the normal stress field in the X, Y and Z directions. As shown in **Fig. 7a**, the maximum von Mises residual stress ($\sigma_{eqv,\ max}$) is 43.75 MPa at node 47 (red zone), and the minimum von Mises residual stress ($\sigma_{eqv,\ min}$) is 0.53 MPa at node 20506 in the apex of the C-ring model (blue zone). As a result, the maximum von Mises residual stress is obtained at two inner edges of the thick zone. The von Mises stress is minimal at the tip of the C-ring because the material is deformed more freely in this area. These calculation results also reflect the stress–strain rule in mechanical theory.

The normal stress field along the X direction (σ_x) is shown in **Fig. 7b**. The maximum tensile normal stress in this direction ($\sigma_{x,\ max}$) is 44.2 MPa at the two inner edges of the thick material area (red zone), and the maximum compressive normal stress value ($\sigma_{x,\ min}$) is -31.55 MPa at node 19808 in the core of the model (blue zone). Compared to the von Mises residual stress field results, the $\sigma_{x,\ max}$ area is similar to the $\sigma_{eqv,\ max}$ area, and the values of $\sigma_{x,\ max}$ are close to the values of $\sigma_{eqv,\ max}$. In particular, the distribution of the von Mises stress field is similar to that of the normal stress in the x-direction.

The normal stress field along the Y direction (σ_y) is illustrated in **Fig. 7c**. The maximum tensile normal stress in the Y direction ($\sigma_{y,\ max}$) is 34.15 MPa in the regions between the two planes of the thick material area (red zone), and the maximum compressive normal stress value ($\sigma_{y,\ min}$) is -24.18 MPa at node 19373 in the core of the model (blue zone). Compared to the von Mises residual stress field results, the $\sigma_{y,\ max}$ zone moves inward in the plane.

The normal stress field along the Z direction (σ_z) is indicated in **Fig. 7d**. The maximum tensile normal stress in the Z direction ($\sigma_{z,\ max}$) is 32.77 MPa at the center body of the sample and concentrated in the thick material area (red area), the maximum compressive normal stress value ($\sigma_{z,\ min}$) is -20.16 MPa at node 17845 in the core of the model (blue zone).

The tangential stress components in planes XY, YZ and ZX are shown in **Fig. 8**. The red area and the blue area represent tensile stress and compressive stress, respectively. The tangential stress components in the XY (τ_{xy}) plane are more significant than those in the YZ (τ_{yz}) and ZX (τ_{zx}) planes. This means that the influence of the tangential stress components in planes YZ and ZX on the equivalent stress (von Mises) is minimal.

(Fig. 8)

Similarly, the stress fields when quenching the C-ring sample in oil are calculated, and the results are shown in **Figs. 9** and **10**.

(Fig. 9)

(Fig. 10)

The obtained results have shown that the stress distribution in the oil-quenched sample is very similar to the stress distribution when the sample is quenched in the 4% PVP-K60 solution. However, the values of the received stress components are slightly different, as shown in **Table 2** below.

(**Table 2)**

The results in **Table 2** show that all residual stress components of the oil-quenched sample are greater than those of the 4% PVP-K60-quenched sample. Thus, if considered in terms of residual stress after quenching, the 4% PVP-K60 solution is better than oil for quenching a C-ring specimen made of 100Cr6 steel.

Development of the stress at the surveyed node

The calculated results were exported and represented in plots to quantitatively study the development of the stress at each position (node) on the model. **Fig. 11** indicates the formation and development of the internal stress components at node 706 (located at the bottom plane, the same as node 47).

It is known that the quenching process means rapidly and continuously cooling the sample in the quenchant. This means that if there is no phase transformation in the material, the sample will continuously shrink after immersion in the quenchant until it is finished. In this way, the stress components will obtain positive or negative values but not of the same magnitude, as shown in **Fig. 11**. However, during the quenching process of 100Cr6 steel, the lattice volume changed during the phase transformation. Therefore, the material will be compressed and tensiled continuously during quenching and the stress components at these locations are continuously reversed, as shown in **Fig. 11.**

(Fig. 11)

As shown in **Fig. 11,** in the first 6.67 seconds, the stress components at node 706 vary on the positive side of the original axis, which means that the metal is compressed. The value of the normal stress component along the X direction (σ_x) is much larger than that of other stress components, so the von Mises stress (σ_{eqv}) depends almost exclusively on σ_x. The maximum normal stress along the X direction ($\sigma_{x,\,max}$) is approximately 290 MPa, and $\sigma_{eqv,\,max}$ is approximately 250 MPa. In the period from 6.67 to 8.33 seconds, all the stress components are reduced sharply to zero, whereas the stress components evolve on the

negative side of the graph axis in the period from 8.33 seconds to 91.67 seconds. The normal stress (σ_x) is still higher than the others and reaches a maximum value ($\sigma_{x,\ max}$) of approximately -405 MPa. The reversed σ_x stress but reduced intensity is observed after 91.67 seconds. The maximum value of the normal stress component in the X direction ($\sigma_{x,\ max}$) after 500 seconds at node 706 is 45.1 MPa, and the maximum von Mises residual stress ($\sigma_{eqv,\ max}$) at node 706 is 43.97 MPa. There are two impact factors on the above results: shrinkage during quenching and expansion due to phase transformation. In the quenching process of the C-ring samples in the 4% PVP-K60 quenchant, the stress components that appear in the 0-500 second range are denoted as the components of the operating stress, and the stress components after finishing quenching for approximately 500 seconds (when the sample was cooled to ambient temperature) are denoted as the components of the residual stress. The intensity of the residual stress is smaller than that of the operating stress.

4.2.3. Distortion of the C-ring samples after quenching

The simulation results of the displacement components of the C-ring samples during quenching in the 4% PVP-K60 quenchant are shown in **Fig. 12.** To clearly show the deformation of the sample before and after quenching, the technique of displaying both the original FEM results concurrently with the calculation results is used. Here, the distribution of the color bands describes the position of the sample after quenching and has been magnified 20 times. The displacement of all the sample nodes in the X direction (the opening direction of the C-ring sample - Gap width) is illustrated in **Fig. 12a**. The observation of the maximum displacement in the X direction is +0.05 mm (red zone) at node 2029 in the apex of the C-ring sample. Since the model's coordinate system is in the center of a large circle, the displacement of node 1964 on the opposite side of node 2029 through the opening is the same as node 2029 with a negative sign (blue area). The difference in the calculated value of the displacement in the X direction of these two nodes is due to an error of calculation. **Fig. 12b** shows the displacement of the sample in the Y direction after quenching in the 4% PVP – K60 quenchant. The maximum displacement value in this direction is 0.074 mm at the C-ring top (node 584).

(Fig. 12)

The displacement of the sample in the Z direction (thickness direction) is shown in **Fig. 12c**. As a result, the displacement of all the nodes in the thickness direction (Z-axis) is relatively small. The total displacement in the 3 directions X, Y and Z is indicated in **Fig. 12d**. In this case, the positions with the largest total displacement ($D_{norm,\ max}$) are the nodes (100; 584;...etc) at the end of the C-ring apex with a displacement value of 0.0816 mm.

The displacement calculation results of the C-ring specimen when quenched in oil are described in **Fig. 13**. The results show that the most significant displacements in the X, Y, and Z directions were 0.053, 0.074, and 0.028 mm, respectively. The total displacement of the oil-quenched C-ring sample was 0.0819 mm. Similar to the 4% PVP-K60 quenchant, when quenching in the oil, the displacement in the Z direction is the smallest in the three directions. Compared with the 4% PVP-K60-quenched sample, the displacement in the X and Z directions and the total displacement of the oil-quenched sample were larger. However, the difference in displacements in the X, Y, and Z directions and the total is small. This result also reflects the law that the 4% PVP-K60-quenched C-ring has a CR_{300} that is smaller than that of the oil-quenched C-ring (**Fig. 4b**), so the distortion of the received sample is smaller, although the CR_{max} of the 4% PVP-K60 quenchant is larger than that of the oil quenchant. Thus, the distortion on the quenched sample largely depends on the CR_{300} or the cooling rate in the austenite to martensite transformation zone.

(Fig. 13)

Development of displacement formation at the surveyed node

To quantitatively investigate the development of the displacement at each node of the model, we exported and presented the calculation results in graph form. The graphs in **Fig. 14** show the displacement component changes at node 584 (at the tip of the model) from the moment the sample was immersed in the 4% PVP-K60 solution until the sample cooled to ambient temperature.

As mentioned above, if there is no phase transformation of the material, the sample will continuously shrink (deform) during quenching from start to finish. In this case, the displacement will only always increase or decrease and will not change, as shown in **Fig. 14**. However, due to the phase transformation during the quenching of the 100Cr6 steel in the 4% PVP-K60 medium, the lattice of the steel volume was changed, so the sample strain was continuous and the displacement components at any position were continuously reversed, as shown in **Fig. 14**.

(Fig. 14)

As shown in **Fig. 14**, the displacement values at node 584 largely increase and decrease continuously in the first 20 seconds. There are two factors that impact these displacements: shrinkage due to quenching and expansion due to phase transformation. After approximately 160 seconds, the displacement components are almost unchanged. The results have

shown that node 584 is displaced by -0.0337 mm, 0.074 mm, -0.0054 mm, and 0.0816 mm in the Dx, Dy, Dz and Dnorm directions, respectively.

The development of the displacement at node 584 during quenching in oil is shown in **Fig. 15**. The results show that the change in the displacement values in the X, Y, Z directions on the oil-quenched sample reflects the same rule as the 4% PVP-K60-quenched sample.

(Fig. 15)

To determine the distortion values of the GW (at locations: top, middle and bottom), ID and OD, the displacement calculation results at nodes 555, 556, 682 and 1292 (**Fig. 16**) need to be extracted.

(Fig. 16)

The displacement values at nodes 584, 555, 556, 682 and 1292 in the X, Y, and Z directions and the total displacement of the two samples quenched in oil and the 4% PVP-K60 solution are listed in **Table 3**. The results show that the oil-quenched sample has displacement values in all directions and that the total displacement is greater than that of the 4% PVP-K60 solution, but the difference is relatively small. The displacement at node 584 is the greatest because the cooling rate at this node is maximal.

(Table 3)

From the displacement in the X direction (Dx) in Column 3 and Column 7 of **Table 3**, the GW, ID and OD values of the C-ring sample were calculated (2 x Dx) and are shown in **Table 4**. According to the deformation results in **Table 4**, it is easy to see that the C-ring samples quenched in oil and 4% PVP-K60 both increase in size after quenching. The highest deformation was observed at the open top (GW) of the C-ring sample, and this behavior was also observed in other studies (Ref 37, 38). The increases in the GW, ID and OD values in this study are related to the formation of the martensite phase at different thick and thin sections on the C-ring sample. The formation of martensite leads to the volume expansion of the material (Ref 38).

(Table 4)

Comparing the openness (GW) of the sample at 3 locations, top, middle, and bottom, it is easy to see that the GW at the top position of the C-ring is the largest because in this position, the cooling rate is the largest. The results in **Table 4** also showed that the openings GW, ID, and OD of the C-ring, when quenched in oil, were greater than those of the C-ring quenched in 4% PVP-K60. The maximum difference in the openings of the C-ring sample when cooled in oil and 4% PVP-K60 was approximately 19%. These results confirm that the 4% PVP-K60 quenchant can replace oil in the quenching of 100Cr6 steel.

4.3. Experimental results

4.3.1 Hardness of the C-ring samples after the quenching

To study the consistency and to facilitate the evaluation, the authors performed microhardness measurements in 2 regions of the sample. One region has a fast cooling rate (thinnest region of C-ring - zone A), and the other has a slow cooling rate (thickest region of C-ring – zone B). At each zone A and B on the sample, the hardness is measured at 5 different locations, and the hardness values reported is the average of the measurement points.

The results of the experimental measurements of hardness are shown in **Table 5**. The oil-quenched sample has a hardness greater than that of the sample quenched in a 4% PVP solution by approximately 3 HV on average. For both samples, the hardness in zone A was higher than that in zone B, which means that the region with the higher cooling rate exhibited the higher hardness. The hardness difference between zones A and B for the samples quenched in oil and 4% PVP-K60 is 10.6 and 11.6 HV, respectively. Thus, although the cooling rates of these regions are larger than the critical cooling rate of 100Cr6 steel, the hardness would be lower at the locations where the cooling rate is lower.

(Table 5)

The results from the comparison of the hardness measured by the experiment with the results obtained from the simulation in Section 4.2.1 are obtained as shown in **Fig. 17**. The results show that the hardness in zone A was greater than that in zone B for both samples quenched in oil and 4% PVP-K60 solution. The hardness in zone A was greater than that in zone B by approximately 2-3 HV. On the other hand, the simulation and experimental results have the largest difference of approximately 4 HV. This shows that the simulation calculation program is meaningful in assessing the hardness of the quenched sample.

(Fig. 17)

4.3.1. Stress values

After the distortion measurements, the sample was subjected to residual stress measurements by X-ray diffraction on a Rigaku D/MAX RAPID II machine. The total residual stress σ_ϕ was measured at two surveyed locations that correspond to node 310 and node 480 in the simulation model (**Fig. 18a)**.

Calculation and determination of surface stress $\boldsymbol{\sigma_\phi}$ according to numerical simulation:

To verify the reliability of the residual stress in the simulation, this result was compared to the experimental value. Since the calculated stresses in the simulation were the three-dimensional stress components, whereas the stress measured by X-ray diffraction was the stress on the surface, the following transformation was performed:

The surface containing node 310 and node 480 is the (x, y) plane of the simulation model, so the stress components include σ_x, σ_y, τ_{xy} and τ_{yx} (**Fig. 18b**). The principal stress components σ_1 and σ_2 in plane (x, y) are obtained as follows:

$$\boldsymbol{\sigma_{1,2}} = \frac{\sigma_x+\sigma_y}{2} \pm \sqrt{\left(\frac{\sigma_x-\sigma_y}{2}\right)^2 + \tau_{xy}^2} \quad (4)$$

$$\sigma_\phi = \overrightarrow{\sigma_1} + \overrightarrow{\sigma_2} \quad (5)$$

So, 1D stress is obtained as follows:

$$\sigma_\phi = \sqrt{\sigma_1^2 + \sigma_2^2} \quad (6)$$

(Fig. 18)

To extract the results of the stress simulation calculation at nodes 310 and 480, the residual stress components at the finished quenching time (t = 500 s) are written in Columns 3, 4, and 5 in **Table 6**. Next, the stress components were used in Equation (4) to determine the principal stress components σ_1 and σ_2 (recorded in Columns 6 and 7 of **Table 6**). Due to $\sigma_1 \perp \sigma_2$, the stress σ_ϕ will be calculated by using Equation (6). The results σ_ϕ of node 310 and node 480 for various quenchants are listed in Column 8 of **Table 6.**

(Table 6)

The simulation results also reflect the same rule as the experimental results, in which the residual stress when quenching the C-ring sample in 4% PVP – K60 and oil quenchants at node 480 are larger than the measured result at node 310. On the other hand, the simulation result is very close to the experiment. Thus, it can be confirmed that the computer software simulation of the quenching process can be used to predict the quenching process before an experiment.

4.3.2. Distortion values

The measurement of the varying dimensions of the C-ring before and after quenching, which are displayed in Fig. 3b, was carried out by a Profile Projector coordinate measuring machine. The measurement results of the distortions (GW, ID, and OD) of the C-ring samples will be compared with the values obtained by the numerical simulation (Tables 7-8), and the errors were estimated as the difference between the measured and simulated distortions.

(Table 7)

(Table 8)

Similar to the simulation, the GW openness is also measured and calculated at the top, middle and bottom positions. The results in Table 7 show that the GW distortion at the top position is the greatest and gradually decreases from the top position to the bottom position of the thinnest part of the C-ring. The ID and OD distortions are much smaller than that of GW. The reason is the difference in cooling rate, which affects the transformation of the austenite phase into martensite between the thinnest and thickest regions on the C-ring sample. The transformation of austenite into martensite will cause volume expansion of the material (Ref 38), and where more martensite is formed (top of the C-ring), there will be more distortion and a higher hardness. The simulation results similarly reflect the aforementioned rule of the experiment. The calculation results in Tables 7-8 also show that the maximum error between the simulation and experiment is 20%, which is acceptable (Ref 22). This means that the simulation results from the program and the computational conditions are entirely usable to predict the distortion of the sample during quenching, thereby allowing for the identification of a suitable quenchant for a particular material with a defined shape and size. Therefore, saving time and reducing testing costs or bringing high economic efficiency in research and production can be realized. In addition, the numerical simulation is significant and effective for new problems (new materials and/or new quenchants).

5. Conclusions

This paper reported the results of the hardness, stress and distortion for C-ring sample quenching in 4% polyvinylpyrrolidone (PVP) – K60 solution and oil by using simulation and experimental measurements. The study showed that the CR_{max} of the 4% PVP-K60 solution was greater than that of the oil, but the cooling rate of the 4% PVP-K60 solution at 300 °C (CR_{300}) was smaller than that of the oil. The greater the CR_{300} was, the greater the hardness, stress, and distortion. The oil-quenched sample had a hardness greater than that of the sample quenched in a 4% PVP solution by approximately 3 HV on average. At the locations where the cooling rate was lower, the hardness was lower. All residual stress components of the oil-quenched sample were greater than those of the 4% PVP-K60-quenched sample. The openness of the GW, ID, and OD of the oil-quenched C-ring sample was larger than that the PVP-K60-quenched C-ring sample, which means that the C-ring sample was more distorted when quenched in oil in comparison with 4% PVP-K60 solution. The values of hardness, stress and distortion of the quenched samples depend less on CR_{max} and more on CR_{300}. Simulation and experimental results of the hardness, stress, and distortion of the C-ring samples reflected the same rule. The errors between the simulation and experiment regarding distortion were approximately 20%. The research results also showed that a solution of 4% PVP-K60 could replace oil for quenching 100Cr6 steel with the aim of reducing distortion and residual stress in the quenched parts, which is environmentally friendly and improves working conditions while still achieving the same hardness results as conventional oil quenching. The application of the computational model in this study has great significance for the heat treatment industries that design of machine parts, the prediction of mechanical properties, and the prevention of failure due to fractures in quenched components. However, for a more comprehensive assessment, further studies are required on the influence of the quenching medium on the microstructure of the steel. Furthermore, the useful lifetime of the 4% PVP-K60 quenchant must also be studied to confirm the significance of this quenching medium.

Acknowledgments

This research is funded by Hanoi University of Science and Technology (HUST) under project number ‘‘T2021-PC-030”

References

[1] Charles E. Bates, George E. Totten and Robert L. Brennan: Heat Treating of Steel, Vol. 4, ASM Handbook Committee, Section 1, (1991), 160.

[2] Z. Li, B. L. Ferguson, X. Sun and P. Bauerle: Proc. 23rd ASM Heat Treat. Soc. Conf., (2005), Pittsburgh, PA, USA.

[3] R.A. Hardin, C. Beckermann: Proc. 59th SFSA Technical and Operating Conference, Chicago, Paper No. 3.3, Steel Founders' Society of America, (2005).

[4] Nicolas Cyril, Baudouin Cyrille, Leleu Stéphane, Teodorescu Mihaela and Bigot Régis: Int J Mater Form, **2** (2009), 263. DOI: 10.1007/s12289-09-0484-y.

[5] G. E. Totten, C. E. Bates and N. A. Clinton: Handbook of Quenchants and Quenching Technology, ASM International, Materials Park, (1993), 35.

[6] Thi Xuan Tran, Xuan Phuong Nguyen, Duong Nam Nguyen, Dinh Toai Vu, Minh Quang Chau, Osamah Ibrahim Khalaf and Anh Tuan Hoang, Effect of Poly-Alkylene-Glycol Quenchant on the Distortion, Hardness, and Microstructure of 65Mn Steel, Computers, Materials & Continua, 2021, DOI:10.32604/cmc.2021.01541.

[7] George E. Totten: Polymer quenchants for induction heat treating applications: The basic, Union Cacbit Corporation 771 Old SawMill River Road Tarrytown, NY 10591, (2000).

[8] M. Eshraghi-Kakhki, M.A. Golozar and A. Kermanpur, Application of polymeric quenchant in heat treatment of crack-sensitive steel mechanical parts: Modeling and experiments, Mater. Des., 2011, https://doi.org/10.1016/j.matdes.2010.12.023.

[9] Z. Koudil, R. Ikkene and M. Mouzali, Cooling Capacity Optimization: Calculation of HardeningPower of Aqueous Solution Based on Poly(N-Vinyl-2-Pyrrolidone), Journal of Materials Engineering and Performance, 2014, DOI: 10.1007/s11665-013-0775-9.

[10] Julinová M, Kupec J, Houser J, Slavík R, Marusincová H and Cervenáková L, Klívar S., Removal of Polyvinylpyrrolidone from Wastewater Using Different Methods, Water Environment Research, 20123, DOI:10.2175/106143012X13373575830999.

[11] Eduardo Vieira, Luciano Volcanoglo Biehl, Jorge Luis Braz Medeiros, Vagner Machado Costa and Rodrigo Jorge Macedo, Evaluation of the characteristics of an AISI 1045 steel quenched in diferent concentration of polymer solutions of polyvinylpyrrolidone, Scientific Reports, 2021, DOI:10.1038/s41598-020-79060-0.

[12] A A Zainulabdeen, N Y Mahmood and J H Mohmmed, The effect of polymeric quenching media on mechanical properties of medium carbon steel, Materials Science and Engineering, 2018, doi:10.1088/1757-899X/454/1/012053.

[13] B. Hernandez-Morales, O. Barba-Mendez, A. Ingalls-Cruz and J. A. Barrera-Godinez, Mathematical modelling of temperature and stress evolution during cooling of a stainless steel Navy C-ring probe, Int. J. Mater. Prod. Techn ol., 2005, https://doi.org/10.1504/IJMPT.2005.007957.

[14] Nailu Chen, Lizhan Han, Weimin Zhang and Xiaowei Hao, Enhancing mechanical properties and avoiding cracks by simulation of quenching connecting rods, Materials Letters, doi:10.1016/j.matlet.2006.10.078.

[15] K. Clemons, C. Lorraine, G. Salgado, A. Taylor, J. Ogren, P. Umin and O.S. Es-Said, Effects of Heat Treatments on Steels for Bearing Applications, JMEPEG, 2007, DOI: 10.1007/s11665-007-9075-6.

[16] Lukasz Rogal, Grzegorz Korpala and Jan Dutkiewicz, Evolution of microstructure in 100CR6 steel after cooling from A thixoforming temperature to bainitic transformation ranges, Materials Science & Engineering A, 2014, http://dx.doi.org/10.1016/j.msea.2014.11.055.

[17] Webster, H., and Laird and W. J.: Martempering of steel, Vol. 4, ASM Handbook Committee (1991), 137.

[18] Chunyan Nan, Derek O. Northwood, Randy J. Bowers and Xichen Sun, Study on the Dimensional Changes and Residual Stresses in Carbonitrided and Ferritic Nitrocarburized SAE 1010 Plain Carbon Steel, Materials Science Forum, 2010, DOI: 10.4028/www.scientific.net/MSF.638-642.829.

[19] Victoria Campagna, Randy Bowers and Derek O. Northwood, Distortion and Residual Stresses in Nitrocarburized and Carbonitrided SAE 1010 Plain Carbon Steel, SAE Int. J. Mater. Manuf., 2008, https://doi.org/10.4271/2008-01-1421.

[20] ESI Groups Sysweld 2017.0 Materials Database - CD Toolbox. 99 Rue Des, Solets Silic 112 94513 Rungis Cedex France, (2017).

[21] Jiang GUO, Haiyang FU, Bo PAN, Renke KANG: Recent Progress of Residual Stress Measurement Methods: A Review, Chinese Journal of Aeronautics, (2019), doi: https://doi.org/10.1016/j.cja.2019.10.010.

[22] Zienkiewicz, O. C.: The Finite Element Method McGraw-Hill, London, (1977).

[23] Bathe, K. J.: Finite Element Procedures in Engineering Analysis, Prentice-Hall, Englewood Cliffs, (1982).

[24] M.E. Fitzpatrick, A.T. Fry, P. Holdway, F.A. Kandil, J. Shackleton and L. Suominen: Determination of residual stresses by x-ray diffraction - Issue 2, Measurement Good Practice Guide No. 52, ISSN 1744-3911, The Controller of HMSO and the Queen's Printer for Scotland, (2005).

[25] Eckehard Mueller, Precision of the Residual Stress determined by X-ray Diffraction: Summery and Limits, 19th International Congress of Metrology, 2019, https://doi.org/10.1051/metrology/201927001.

[26] K. Bobz, W. Wietheger, M. A. Knoch, A. Schacht, U. Reisgen, R. Sharma and L. Oster, Comparison of Residual Stress Measurements Conducted by Xray Stress Analysis and Incremental Hole Drilling Method, J Therm Spray Tech, 2020, https://doi.org/10.1007/s11666-020-01056-z

[27] Prevéy, Paul S., X-ray Diffraction Residual Stress Techniques, Metals Handbook. 10. Metals Park: American Society for Metals, (1986), 380.

[28] Marlon Muniz Nunesa , Eduardo Miguel da Silvab, Reny Angela Renzettia, Tarcisio Gonçalves Britoa, Analysis of Quenching Parameters in AISI 4340 Steel by Using Design of Experiments, Materials Research, 2019, DOI: http://dx.doi.org/10.1590/1980-5373-MR-2018-0315.

[29] A.D. da Silva, T.A. Pedrosa, J.L. Gonzalez-Mendez, X. Jiang, P.R. Cetlin, T. Altan, Distortion in quenching an AISI 4140 C-ring – Predictions and experiments, 2012, https://doi.org/10.1016/j.matdes.2012.05.031.

[30] M. Manivannan, D. O. Northwood & V. Stoilov, Use of Navy C-rings to study and predict distortion in heat treated components: experimental measurements and computer modelling, International Heat Treatment and Surface Engineering, 2014, http://dx.doi.org/10.1179/1749514814Z.000000000119.

[31] E. Troell, H. Kristoffersen, ... S. Segerberg, Thermal Engineering of Steel Alloy Systems, Comprehensive Materials Processing, (2014), 99.

[32] Brimacombe, J.K., S.M. Gupta, and E.B. Hawbolt , Determination of Quench Heat-Transfer Coefficients Using Inverse Methods, in Proceedings from the First 74 International Conference on Quenching and Control of Distortion, Chicago, Illinois, (1992).

[33] Mills, A.F., Heat Transfer. 2nd Ed ed., “Upper Saddle River”, NJ: Prentice Hall, (1999).

[34] J. P. Holman, “Heat Transfer”, McGraw-Hill, Inc, (2004).

[35] F. Kreith, “Mechanical Engineering Handbook”, CRC Press LLC (1999).

[36] Totten GE. Steel Heat Treatment: Metallurgy and Technologies. 2nd ed. Boca Raton: CRC Press, (2006).

[37] Civera C, Rivolta B, Simencio-Otero RL, Lúcio JG, Totten GE, Canale LC, Vegetable Oils as Quenchants for Steels: Residual Stresses and Dimensional Changes, Materials Performance and Characterization, 2014, DOI:10.1520/MPC20140039.

[38] Feng YY, Xu C, Su X, Sun YL, Pan X, Cao YD, et al., Inflence of austenization temperature on microstructure and mechanical properties of a new ultra-high strength low alloyed steel, Materials Testing, 2017, https://doi.org/10.3139/120.111103.

Figure Caption

Fig. 1 Dimensions [mm] of the C-ring (a) and the finite element model of the C-ring sample (b)

Fig. 2 Thermal convection surface (skin) to the quenchant (a) and the function of the HTC of 4 % PVP-K60 and oil quenchants (b)

Fig. 3 The clamped position of the C-ring sample during quenching (a) and C-ring before heat treatment (n, m, a dimension) and after the quenching (n', m', a' dimension) (b)

Fig. 4 The cooling curves have been recorded using a test probe of Inconel 600, ø12.5 × 60 mm, according to ISO 9950 (a) and cooling rate (b) of 4 % PVP-K60 and oil quenchants

Fig. 5 Hardness of the C-ring specimen when quenched in 4 % solution of PVP-K60 and oil

Fig. 6 CCT diagram of 100Cr6 steel [20]

Fig. 7 Von Mises residual stress field (a) and normal stress in the X direction (b), Y direction (c) and Z direction (d) after the quenching in 4 % PVP-K60 for 500 seconds

Fig. 8 The stress fields in planes XY (a), YZ (b) and ZX (c) after the quenching in 4 % PVP-K60 for 500 seconds

Fig. 9 Von Mises residual stress field (a) and normal stress in the X direction (b), Y direction (c) and Z direction (d) after the quenching in oil for 500 seconds

Fig. 10 The stress fields in planes XY (a), YZ (b) and ZX (c) after the quenching in oil for 500 seconds

Fig. 11 Development of the stress components at node 706 during the quenching in 4 % PVP-K60

Fig. 12 Displacement of the 4 % PVP- quenched sample in the following directions: X (a), Y (b), Z (c) and total distortion (d)

Fig. 13 Displacement of the oil - quenched sample in the following directions: X (a), Y (b), Z (c) and total distortion (d)

Fig. 14 Development of the displacement at node 584 during the quenching in 4 % PVP-K60

Fig. 15 Development of the displacement at node 584 during the quenching in oil

Fig. 16 Location of displacement survey nodes on the model

Fig. 17 Hardness on sample after the quenching in oil and 4% PVP at zones A and B by the simulation and experiment

Fig. 18 Survey of locations of the residual stress on the C-ring (a) and the principal stress components (b)

Table caption

Table 1. Input parameters in the quenching process for the C-ring sample of 100Cr6 steel

Table 2. The maximum value of the stress components when the C-ring sample was quenched in oil and 4 % PVP-K60

Table 3. Displacement in the following directions at nodes of the C-rings when quenched sample in 4 % PVP solution and oil

Table 4. Results of distortion for the quenched C-rings

Table 5. Vickers hardness [Kg/mm^2] at the measurement zones on the sample when quenched in oil and 4 % PVP-K60

Table 6. The residual stress at N310 and N480 on the surface of the C-ring sample of 100Cr6 steel after the quenching in 4 % PVP – K60 and oil quenchants

Table 7. Comparison of measured and predicted GW distortion of C-ring in different quenchants

Table 8. Comparison of measured and predicted distortion of C-ring in different quenchants

Table 1. Input parameters in the quenching process for the C-ring sample of 100Cr6 steel

Parameters	***Values***
Model type	3D (Solid)
Material	100Cr6
Quenchants	4% PVP-K60 and oil
Ambient temperature	25 [^{o} C]
Holding time	500 [s]
Time increments	0.01 ÷ 0.1 [s]
The temperature of the sample	850 [^{o} C]
Time of clamping	500 [s]

Table 2. The maximum value of the stress components when the C-ring sample was quenched in oil and 4 % PVP-K60

Quenching medium	σ_{eqv} [MPa]	σ_x [MPa]	σ_y [MPa]	σ_z [MPa]	τ_{xy} [MPa]	τ_{yz} [MPa]	τ_{zx} [MPa]
Oil	49.5119	48.9752	40.4211	37.2661	22.7956	10.8906	8.24262
4 % PVP –K60	44.5146	45.4787	34.9313	33.988	19.0243	9.84368	7.13926

Table 3. Displacement in the following directions at nodes of the C-rings when quenched sample in 4 % PVP solution and oil

Nodes	**4 % PVP-K60 quenchant**				**Oil quenchant**			
	D_{norm} (mm)	D_x (mm)	D_y (mm)	D_z (mm)	D_{norm} (mm)	D_x (mm)	D_y (mm)	D_z (mm)
584	0.0816	-0.0487	0.0721	-0.0054	0.0819	-0.0492	0.0741	-0.0055
555	0.0761	-0.0315	0.0691	-0.0034	0.0776	-0.0305	0.0712	-0.0052
556	0.0725	-0.0275	0.0669	-0.0049	0.07434	-0.0269	0.06895	-0.0047
682	0.0289	-0.0102	0.0235	-0.0134	0.0316	-0.0118	0.0266	-0.0122
1292	0.0027	-0.0077	0.0027	-0.0174	0.0199	-0.0095	0.0043	-0.0169

Table 4. Results of distortion for the quenched C-rings

Quenchants	**GW** (mm)			**ID** (mm)	**OD** (mm)
	Top	Middle	Bottom		
4 % PVP-K60	0.0974	0.063	0.055	0.0204	0.0154
Oil	0.0984	0.061	0.0538	0.0236	0.019

Table 5. Vickers hardness [Kg/mm^2] at the measurement zones on the sample when quenched in oil and 4 % PVP-K60

No.	Oil		4 % PVP-K60	
	Zone A	Zone B	Zone A	Zone B
1	791	774	785	762
2	787	779	781	773
3	784	775	783	779
4	781	780	790	778
5	794	776	781	770
Average	787.4	776.8	784	772.4

Table 6. The residual stress at N310 and N480 on the surface of the C-ring sample of 100Cr6 steel after the quenching in 4 % PVP – K60 and oil quenchants

Quenchants	Node	σ_x	σ_y	τ_{xy}	σ_1	σ_2	σ_ϕ		Error (%)
							Measurement	Simulation	
4 % PVP-K60	310	10.0	7.2	2.8	11.73	5.47	14.36	12.94	10%
	480	27.82	32.33	0.14	32.33	27.82	48.76	42.65	12.5%
Oil	310	11.2	8.85	3.3	13.53	6.52	18.09	15.02	17%
	480	32.71	37.1	0.05	37.1	32.71	48.76	49.46	1.4%

Table 7. Comparison of measured and predicted GW distortion of C-ring in different quenchants

Quenchants	Measured GW distortion/mm			Predicted GW distortion/mm			Error (%)		
	Top	Middle	Bottom	Top	Middle	Bottom	Top	Middle	Bottom
Oil	0.123	0.0746	0.0654	0.0984	0.061	0.0538	20	18	17
4% PVP-K60	0.118	0.0716	0.0624	0.0974	0.063	0.055	17	12	12

Table 8. Comparison of measured and predicted distortion of C-ring in different quenchants

Quenchant	Measured distortion/mm		Predicted distortion/mm		Error (%)	
	ID	OD	ID	OD	ID	OD
4% PVP-K60	0.023	0.018	0.0204	0.0154	11	14
Oil	0.026	0.021	0.0236	0.019	17	10

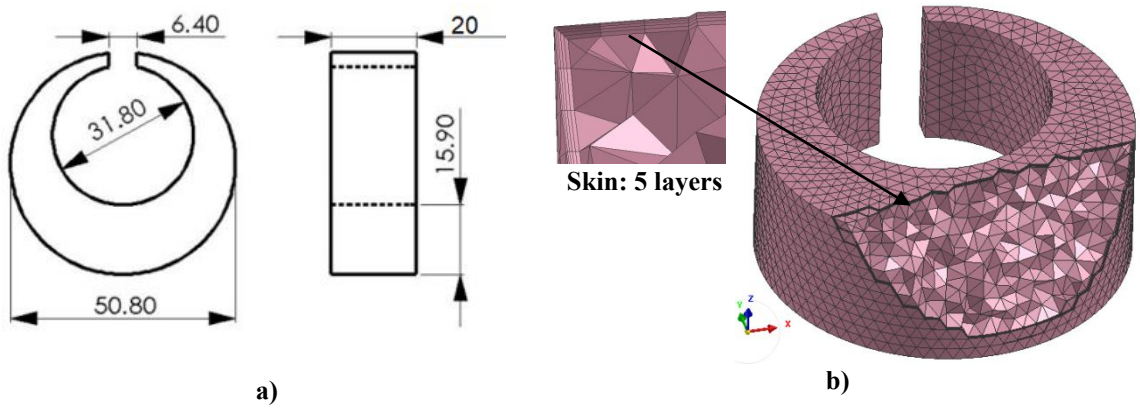

Fig. 1 Dimensions [mm] of the C-ring (a) and the finite element model of the C-ring sample (b)

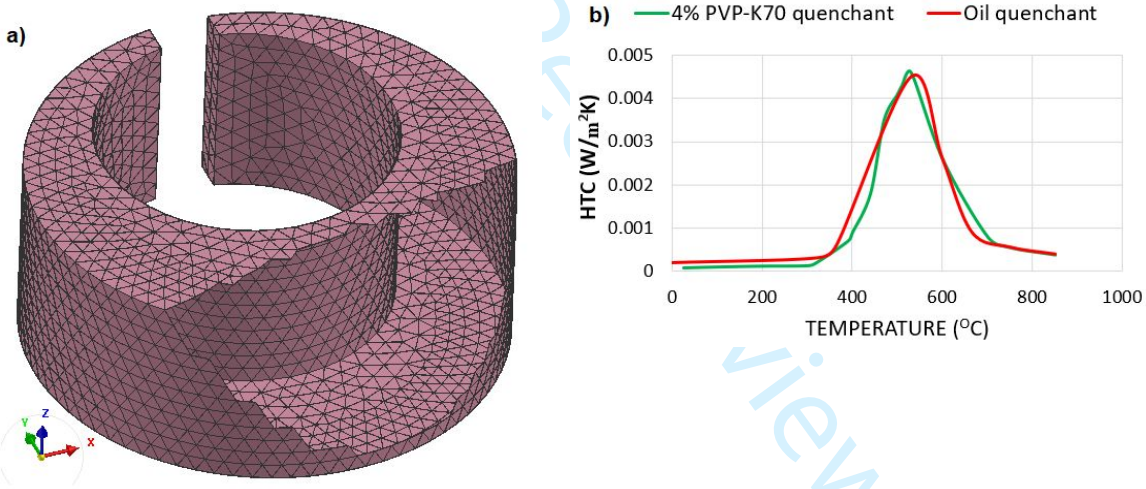

Fig. 2 Thermal convection surface (skin) to the quenchant (a) and the function of the HTC of 4 % PVP-K60 and oil quenchants (b)

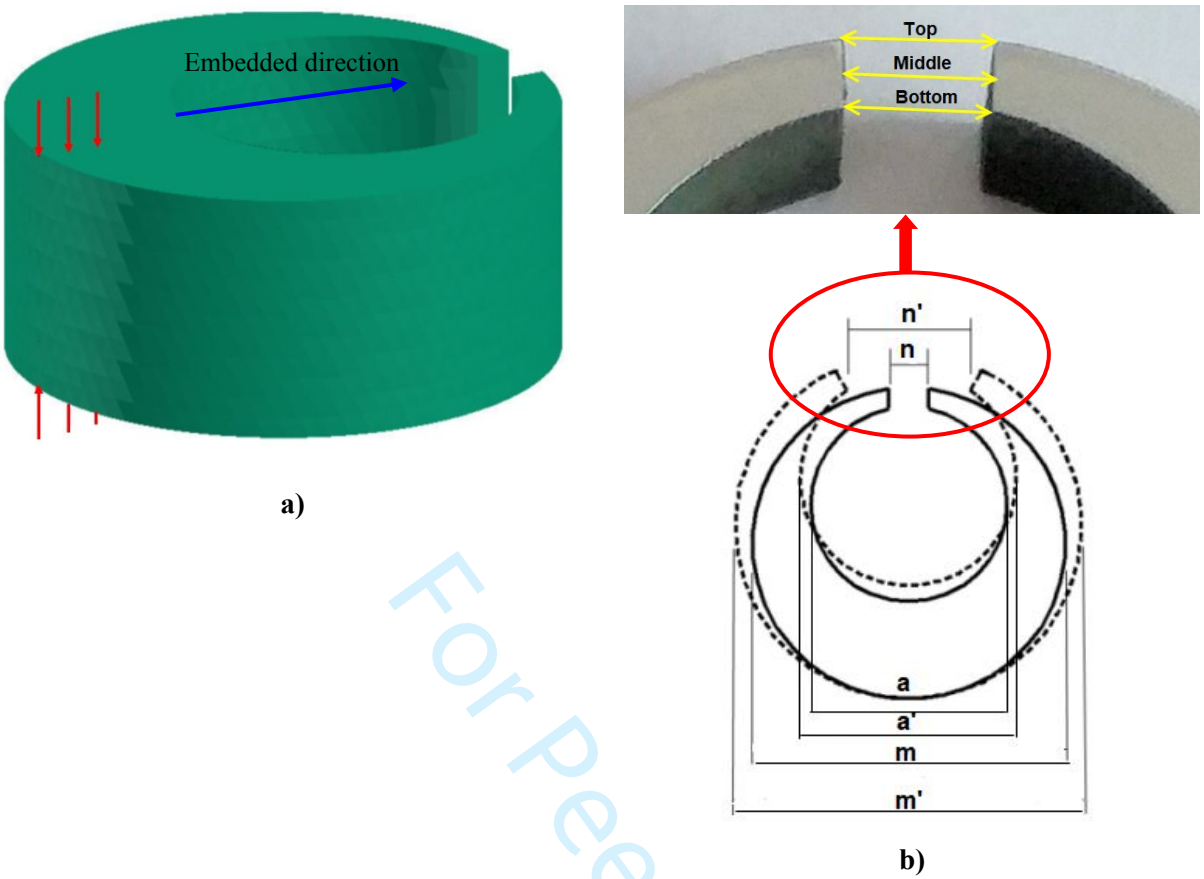

Fig. 3 The clamped position of the C-ring sample during quenching (a) and C-ring before heat treatment (n, m, a dimension) and after the quenching (n', m', a' dimension) (b)

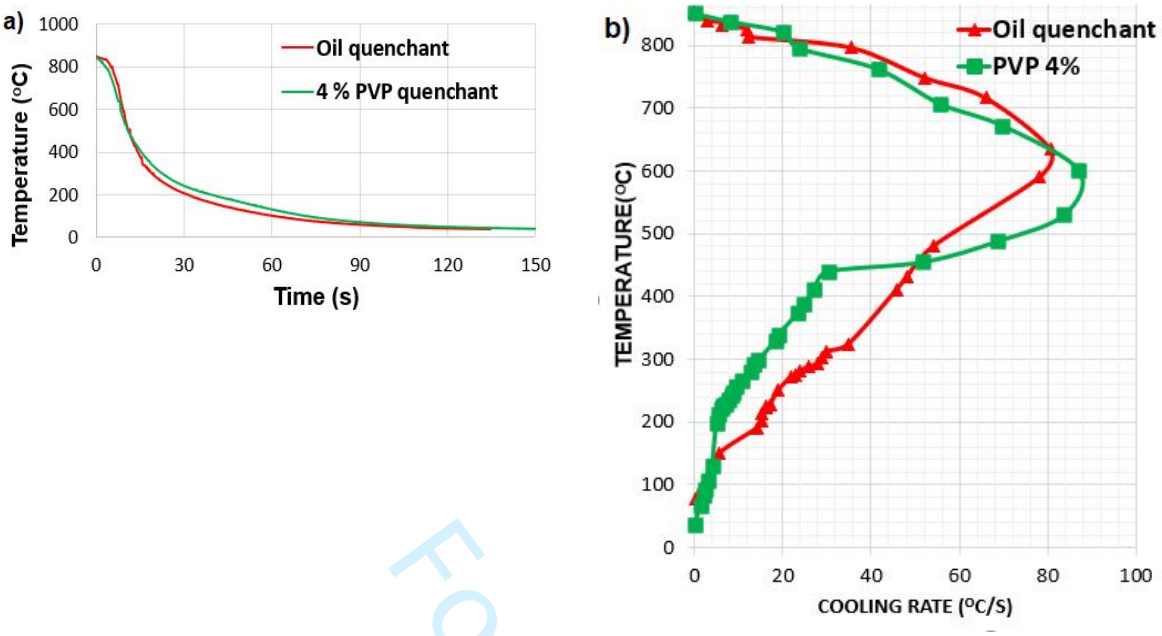

Fig. 4 The cooling curves have been recorded using a test probe of Inconel 600, ø12.5 × 60 mm, according to ISO 9950 (a) and cooling rate (b) of 4 % PVP-K60 and oil quenchants

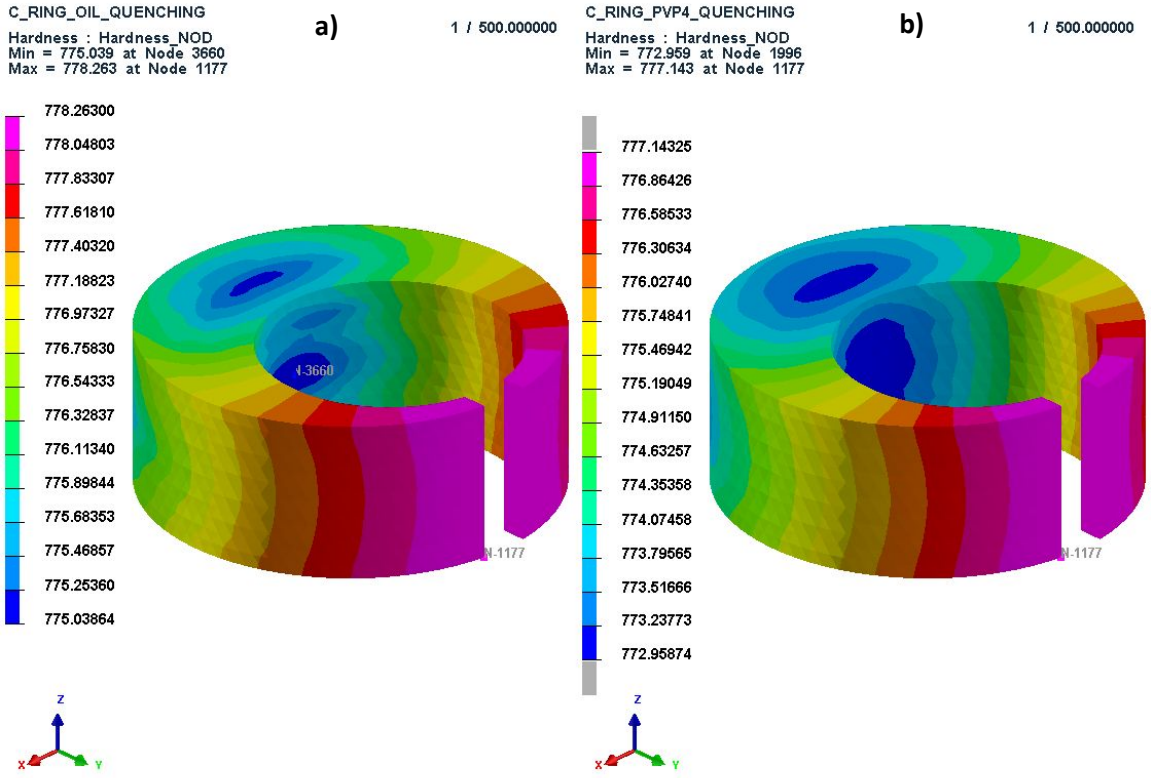

Fig. 5 Hardness of the C-ring specimen when quenched in oil (b) and 4 % solution of PVP-K60 (b) **(Fig. 5)** - *Online version in color*

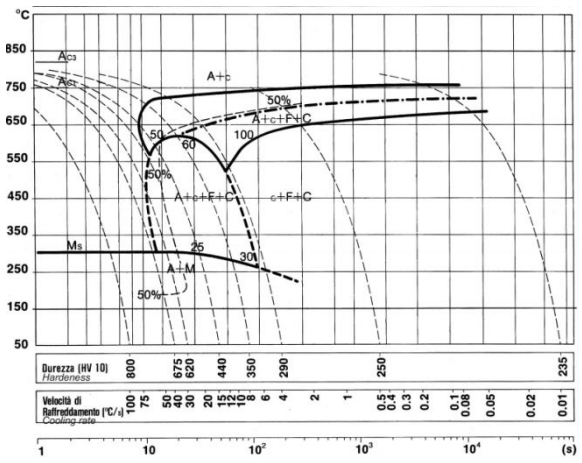

Fig. 6 CCT diagram of 100Cr6 steel (Ref 20)

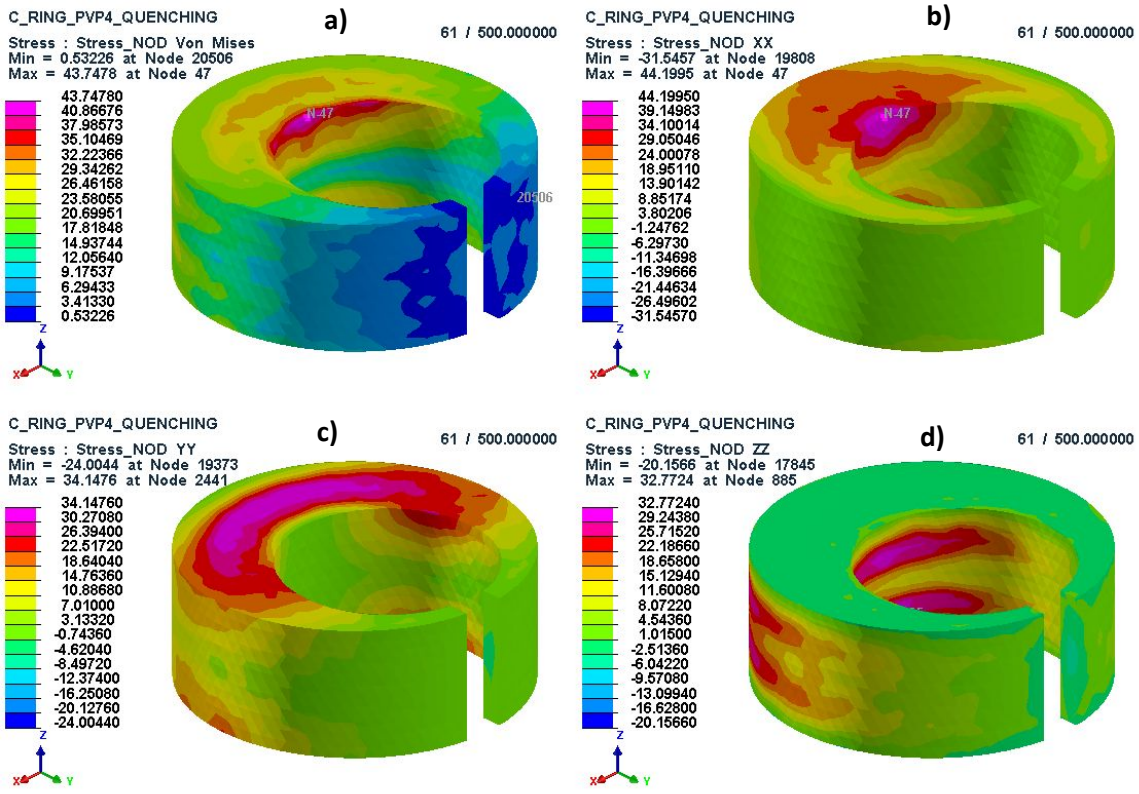

Fig. 7 Von Mises residual stress field (a) and normal stress in the X direction (b), Y direction (c) and Z direction (d) after the quenching in 4 % PVP-K60 for 500 seconds

(Fig. 7) *- Online version in color*

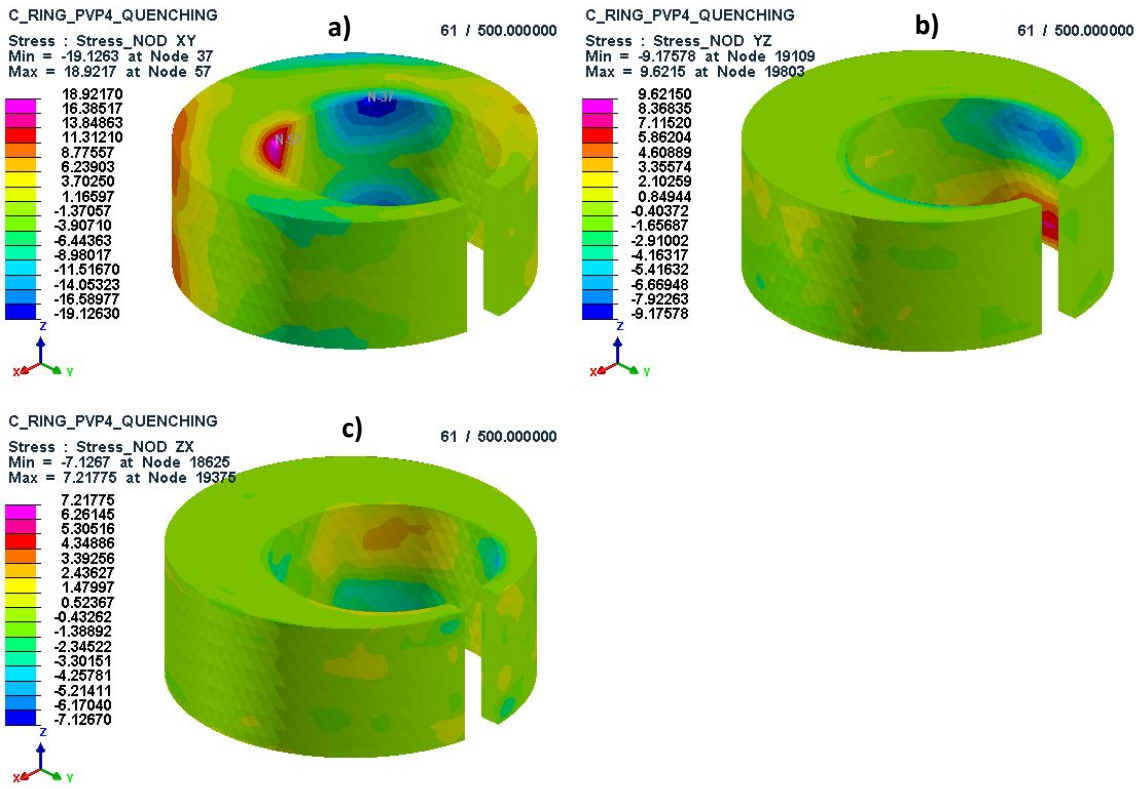

Fig. 8 The tangential stress fields in planes XY (a), YZ (b) and ZX (c) after the quenching in 4 % PVP-K60 for 500 seconds

(Fig. 8) *- Online version in color*

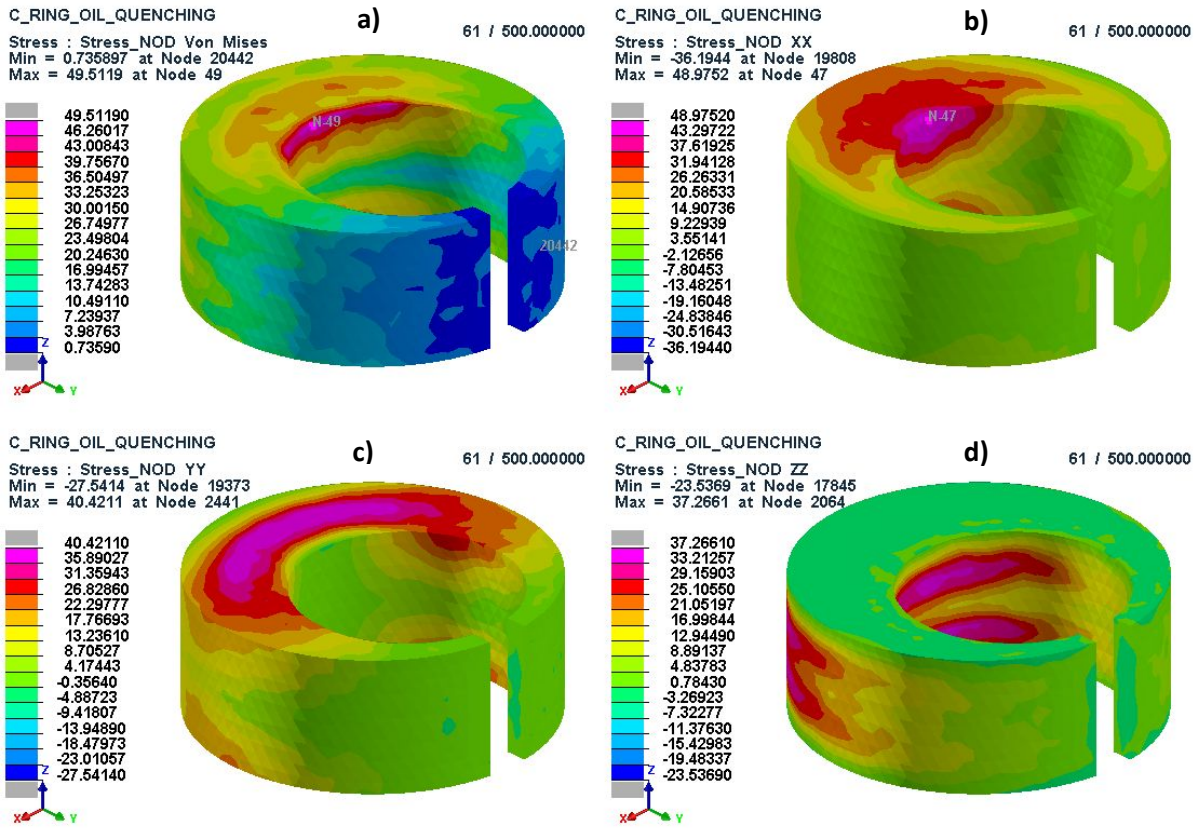

Fig. 9 Von Mises residual stress field (a) and normal stress in the X direction (b), Y direction (c) and Z direction (d) after the quenching in oil for 500 seconds

(Fig. 9) *- Online version in color*

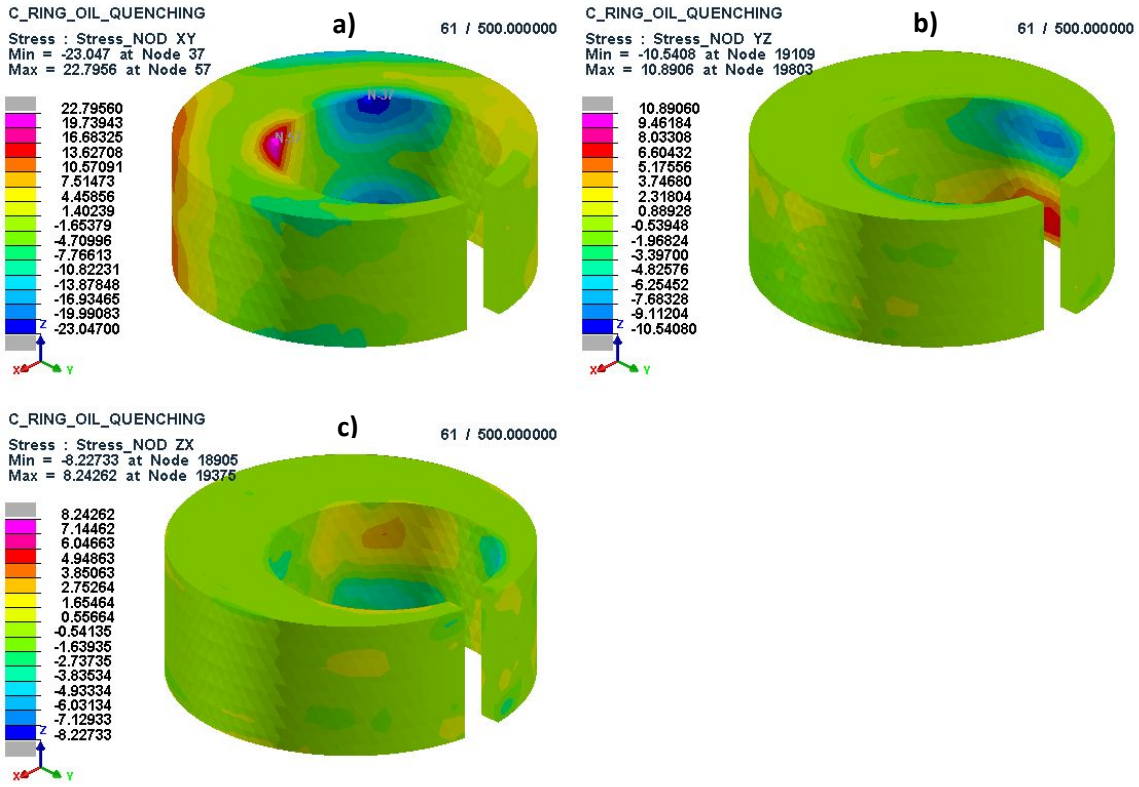

Fig. 10 The tangential stress fields in planes XY (a), YZ (b) and ZX (c) after the quenching in oil for 500 seconds

(Fig. 10) *- Online version in color*

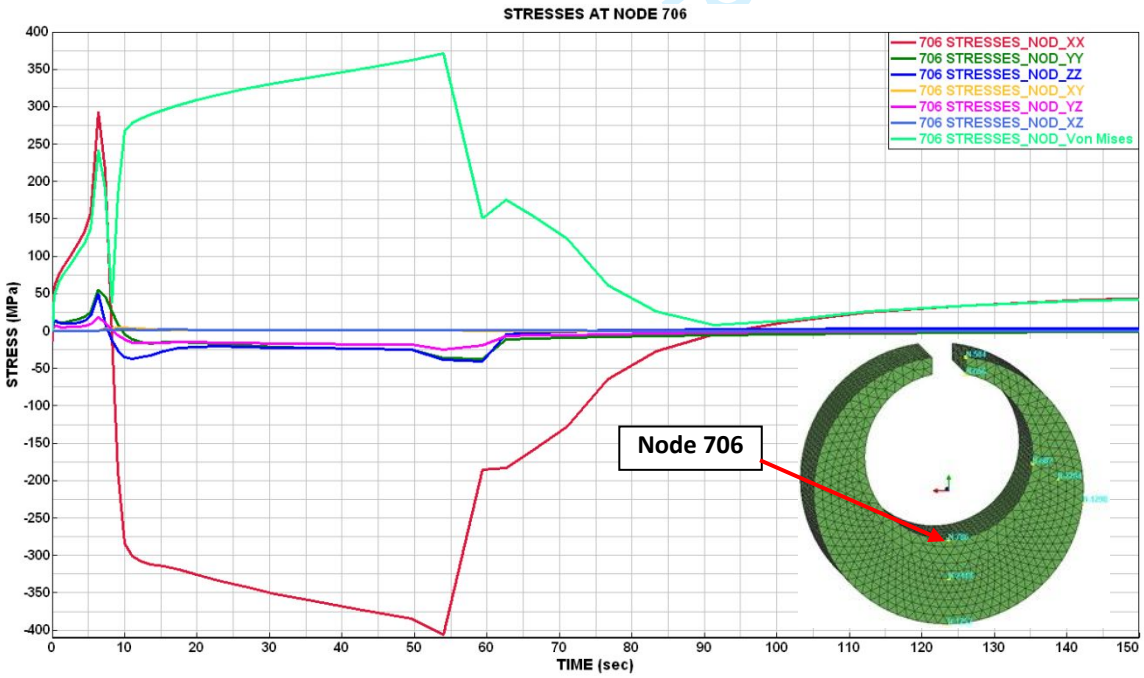

Fig. 11 Development of the stress components at node 706 (or node 47) during the quenching in 4 % PVP-K60

(Fig. 11) *- Online version in color*

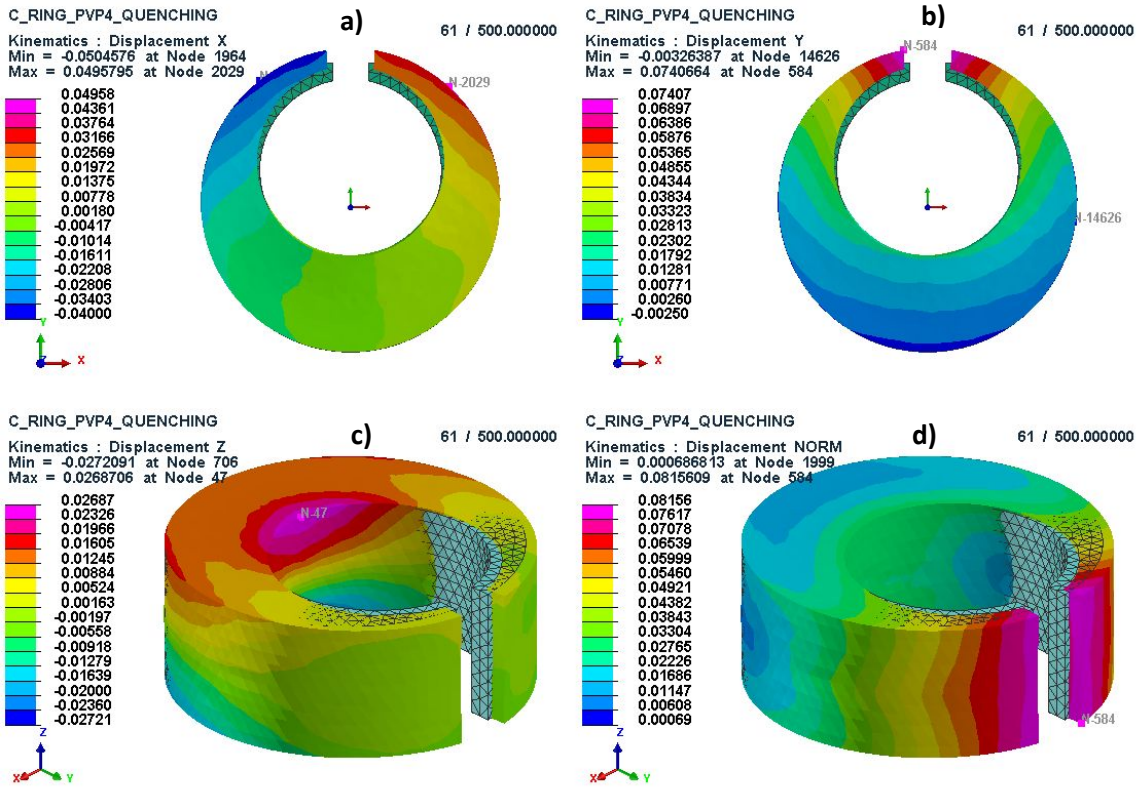

Fig. 12 Displacement of the 4 % PVP-quenched sample in the directions: X (a), Y (b), Z (c) and total distortion (d)

(Fig. 12) *- Online version in color*

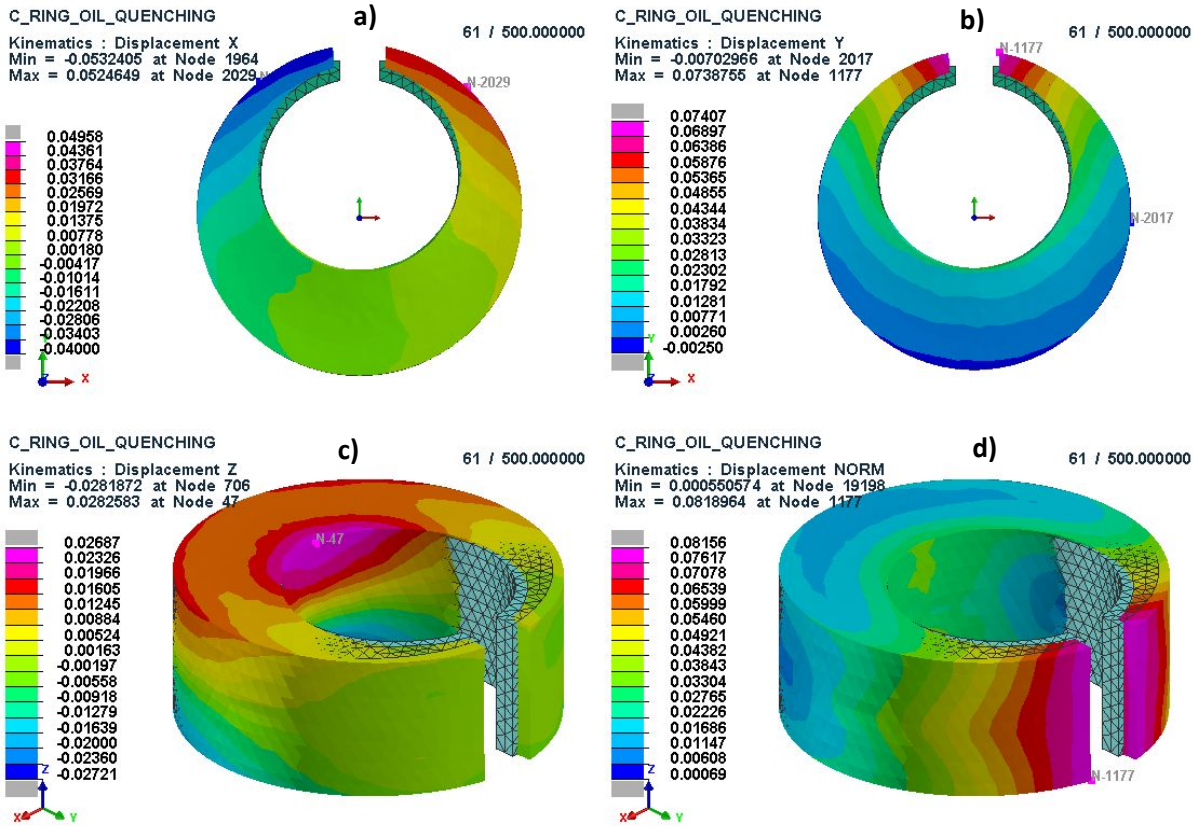

Fig. 13 Displacement of the oil-quenched sample in the following directions: X (a), Y (b), Z (c) and total distortion (d)

(Fig. 13) *- Online version in color*

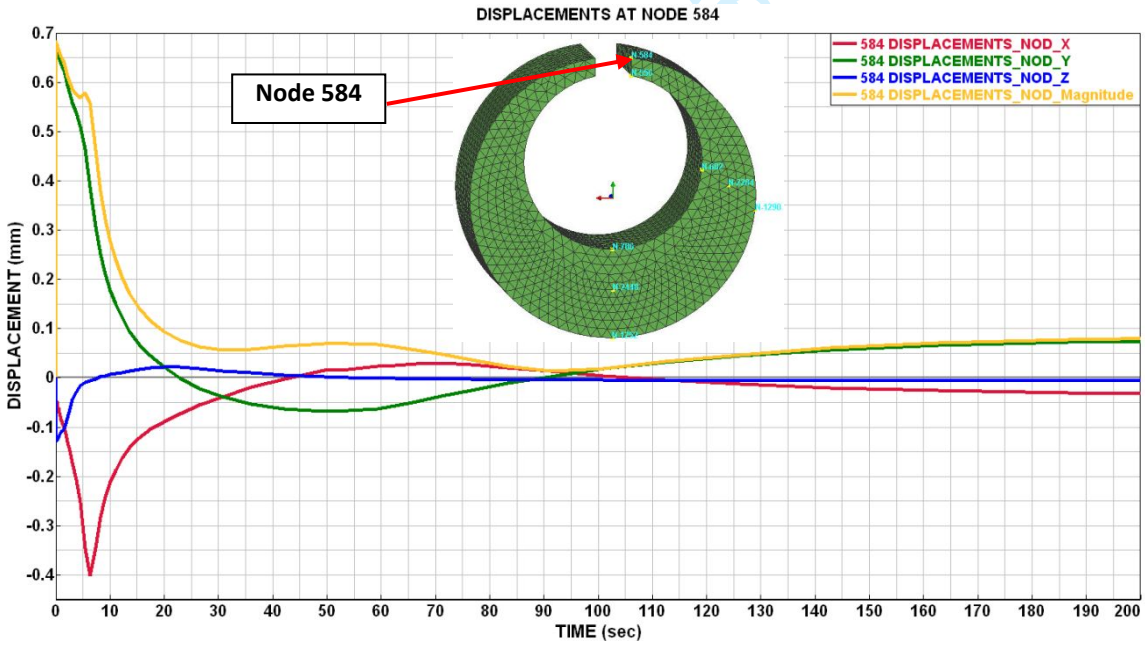

Fig. 14 Development of the displacement at node 584 during the quenching in 4 % PVP-K60

(Fig. 14) *- Online version in color*

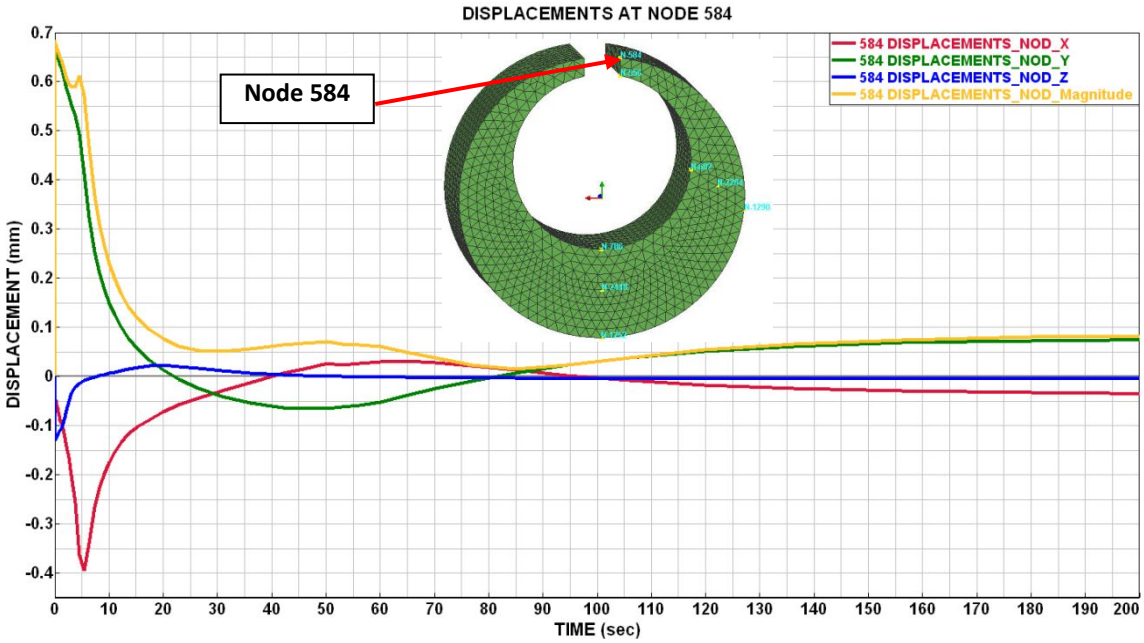

Fig. 15 Development of the displacement at node 584 during the quenching in oil

(Fig. 15) *- Online version in color*

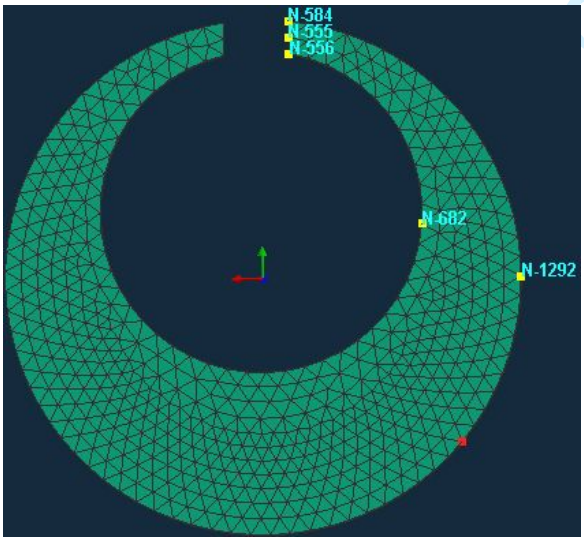

Fig. 16 Location of displacement survey nodes on the model

(Fig. 16) *- Online version in color*

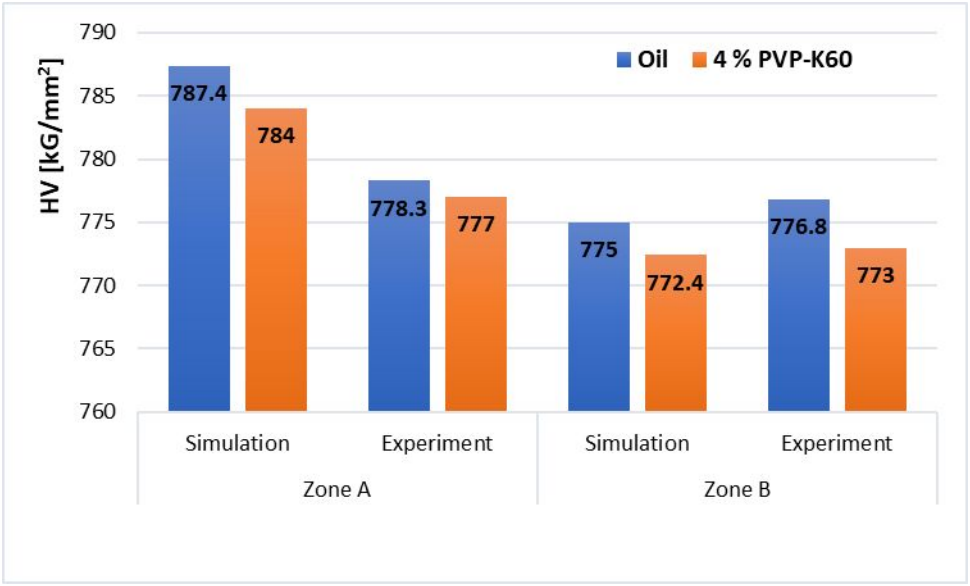

Fig. 17 Hardness on sample after the quenching in oil and 4% PVP at zones A and B by the simulation and experiment

(Fig. 17) *- Online version in color*

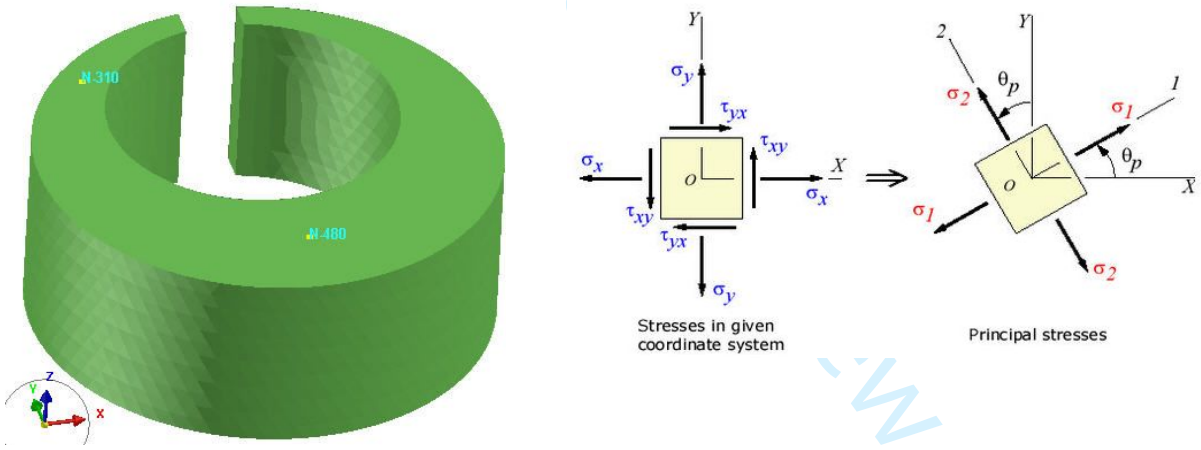

Fig. 18 Survey locations of the residual stress on the C-ring (a) and the principal stress components (b)

(Fig. 18) *- Online version in color*

Editing Certificate

This document certifies that the manuscript

Stress and distortion of 100Cr6 steel after quenching in aqueous 4% polyvinylpyrrolidone solution

prepared by the authors

Xuan Thi Tran, Anh Hoang Pham, Vuong Van Hoang, Toai Dinh Vu*

was edited for proper English language, grammar, punctuation, spelling, and overall style by one or more of the highly qualified native English speaking editors at AJE.

This certificate was issued on **January 24, 2022** and may be verified on the AJE website using the verification code **F26D-5AE2-57F8-828B-5F80** .

Neither the research content nor the authors' intentions were altered in any way during the editing process. Documents receiving this certification should be English-ready for publication; however, the author has the ability to accept or reject our suggestions and changes. To verify the final AJE edited version, please visit our verification page at aje.com/certificate. If you have any questions or concerns about this edited document, please contact AJE at support@aje.com.